Science
AAAS

Coupling of CO2 and Ice Sheet Stability Over Major Climate Transitions of the Last 20 Million Years

Aradhna K. Tripati, *et al.*

Science **326**, 1394 (2009);
DOI: 10.1126/science.1178296

Science (print ISSN 0036-8075; online ISSN 1095-9203) is published weekly, except the last week in December, by the American Association for the Advancement of Science, 1200 New York Avenue NW, Washington, DC 20005.

Coupling of CO_2 and Ice Sheet Stability Over Major Climate Transitions of the Last 20 Million Years

Aradhna K. Tripati,[1,2]* Christopher D. Roberts,[2] Robert A. Eagle[3]

The carbon dioxide (CO_2) content of the atmosphere has varied cyclically between ~180 and ~280 parts per million by volume over the past 800,000 years, closely coupled with temperature and sea level. For earlier periods in Earth's history, the partial pressure of CO_2 (pCO_2) is much less certain, and the relation between pCO_2 and climate remains poorly constrained. We use boron/calcium ratios in foraminifera to estimate pCO_2 during major climate transitions of the past 20 million years. During the Middle Miocene, when temperatures were ~3° to 6°C warmer and sea level was 25 to 40 meters higher than at present, pCO_2 appears to have been similar to modern levels. Decreases in pCO_2 were apparently synchronous with major episodes of glacial expansion during the Middle Miocene (~14 to 10 million years ago) and Late Pliocene (~3.3 to 2.4 million years ago).

The response of ice sheets and climate to past and future changes in the partial pressure of CO_2 (pCO_2) remains uncertain (*1*). Geologic data can be used to constrain relations between pCO_2 and ice sheet stability, identify climate thresholds, and validate models used for simulating future climate change (*1*). Over the past 20 million years (My), there have been substantial changes in global sea level driven by the growth and decay of continental ice sheets. Among the most pronounced of these fluctuations are the growth of ice on East and West Antarctica, the formation of an Arctic ice cap in the Middle Miocene [~14 to 10 million years ago (Ma)], and the intensification of glaciation in the Northern Hemisphere during the Late Pliocene (~3.4 to 2.4 Ma) (*2*–*4*). The causes of these glacial transitions, however, are the subject of intense debate. Proposed mechanisms include changing ocean circulation due to the closure of the Panamanian Seaway (*5*), upper water-column stratification in the tropics and/or high latitudes (*6*), and orbitally driven variations in the amount or distribution of insolation (*2*). Other authors invoke pCO_2 changes to explain glacial expansion (*7*–*9*).

Although there is speculation about the role of the carbon cycle in driving these well-studied climate changes, there is surprisingly little direct evidence to support a coupling between pCO_2 and climate before the ice core record (i.e., before 0.8 Ma). Estimates of pCO_2 for the past 20 My have been generated with the use of several methods (*10*–*13*), including the difference in the carbon isotopic composition ($\delta^{13}C$) of alkenones and co-occurring foraminifera, $\delta^{13}C$ of bulk carbon and pedogenic carbonates, boron isotope composition ($\delta^{11}B$) of foraminifera, stomatal density on fossil leaves, and carbon-cycle modeling. Most reconstructions support a decoupling between pCO_2 (*10*–*13*) and climate (*14*) during the Miocene and Late Pliocene, although very little pCO_2 data are available, and the few published proxy reconstructions yield conflicting results. In addition, few pCO_2 proxies have replicated the ice core data of the past 0.8 My.

To test the hypothesis that CO_2 and climate were closely coupled across these major transitions, we calculated surface-water pCO_2 (and pH) for three intervals [(i) 20 to 5 Ma, (ii) 3.5 to 2.4 Ma, and (iii) 1.4 Ma to the present] using foraminiferal B/Ca ratios. Yu *et al*. demonstrated that planktic foraminiferal B/Ca ratios can be used to estimate seawater borate/bicarbonate ratios [$B(OH)_4^-/HCO_3^-$] (*15*). Seawater $B(OH)_4^-/HCO_3^-$ will respond to changes in the carbonate system (such as pH, alkalinity, or dissolved inorganic carbon), as well as the total concentration of dissolved boron. To calculate pCO_2 and pH from seawater $B(OH)_4^-/HCO_3^-$, Yu *et al*. assumed alkalinity scaled either with surface-water salinity or whole-ocean salinity and total boron concentrations scaled with salinity. The choice of either of these models had a negligible effect on the reconstruction [<10 parts per million by volume (ppmv)].

We reconstructed surface-water $B(OH)_4^-/HCO_3^-$ at sites 806 and 588 located in the western tropical Pacific Ocean (fig. S1). Surface-water pCO_2 at these sites should reflect atmospheric pCO_2, as today this region is close to equilibrium with the atmosphere (table S2), not strongly affected by upwelling, and characterized by low productivity. Although ocean stratification has probably changed over the past 20 My, the western tropical Pacific probably experienced much smaller fluctuations than other regions (the eastern sides of ocean basins, mid-latitude settings, high-latitude settings) (*6*, *16*, *17*). Surface temperatures in this region are also thought to have been relatively stable over long time scales (*18*, *19*), with fluctuations of <6°C, in contrast to other areas (*16*, *17*). Both sites were drilled in shallow waters (table S1), with well-preserved planktonic foraminifera (*10*, *17*–*20*).

We measured B/Ca ratios, Mg/Ca ratios, and $\delta^{18}O$ values in monospecific samples of the surface-dwelling species *Globigerinoides ruber* and *G. sacculifer* (tables S3 and S4). Average reproducibility for B/Ca ratios of separately cleaned samples was 3.5%. B/Ca ratios were converted to seawater $B(OH)_4^-/HCO_3^-$ ratios with the use of an appropriate value for the apparent partition coefficient (K_D). K_D was calculated for each sample by applying a species-specific calibration between K_D and temperature (table S7) to Mg/Ca-derived estimates of temperature. Calculated $B(OH)_4^-/HCO_3^-$ ratios (and pCO_2 values) for 20 replicates typically differ by less than 4% (table S8), and values calculated using 78 pairs of *G. ruber* and *G. sacculifer* from the same sample agreed to within 3%, on average (table S9) (*21*).

To estimate pH and pCO_2 from $B(OH)_4^-/HCO_3^-$ ratios, a further assumption is required to fully constrain the carbonate system. We use seawater $B(OH)_4^-/HCO_3^-$ ratios and estimates of alkalinity or carbonate ion concentration to determine pH and pCO_2 [section F of supporting online material (SOM)]. We tested the sensitivity of calculated pH and pCO_2 values to the assumption used, including the following assumptions: (i) alkalinity scaled with salinity, (ii) constant carbonate ion concentration, and (iii) variable carbonate ion concentration. Seawater B has an oceanic residence time of ~11 to 17 My (*22*). Although we do not know how seawater B has evolved over the past 20 My, variations in seawater $B(OH)_4^-/HCO_3^-$ ratios on time scales of a few million years should reflect changes in the seawater carbonate system. We assumed total B (fig. S7) may have followed one of five modeled histories (*22*). The equations that we used for our calculations are provided in sections G to I of the SOM.

In total, we used 28 models to calculate pH and pCO_2 from $B(OH)_4^-/HCO_3^-$ ratios (figs. S5 to S8 and table S12). The range of calculated values defines the shaded regions in Figs. 1 and 2. The variable alkalinity model is shown in Figs. 1 and 2 (gray and green circles), because it is typically within 5 ppmv of the average of all 28 models. pCO_2 values calculated using the 28 models agree to within 40 ppmv over the last 800 thousand years (ky), with the difference between minimum and maximum calculated values increasing farther back in time (50 ppmv from 0 to 5 Ma, 60 ppmv from 5 to 10 Ma, and 100 ppmv from 10 to 20 Ma).

The pCO_2 reconstruction accurately reproduces ice core measurements from 0 to 0.8 Ma (Fig. 1). If the variable-alkalinity model is considered (Fig. 1, gray circles), ~30- to 50-ppmv offsets are observed for three (of 41) samples, which may be due to differences in age models [128 and 374 thousand years ago (ka)] or inaccuracies in the reconstruction (at 581 ka). For

[1]Departments of Earth and Space Sciences and Atmospheric and Oceanic Sciences, and Institute of Geophysics and Planetary Physics, University of California, Los Angeles (UCLA), Los Angeles, CA 90095, USA. [2]Department of Earth Sciences, University of Cambridge, Cambridge, CB2 3EQ, UK. [3]Division of Geological and Planetary Sciences, California Institute of Technology, Pasadena, CA 91125, USA.

*To whom correspondence should be addressed. E-mail: ripple@zephyr.ess.ucla.edu

the whole population of pCO_2 estimates from this interval (n = 39 samples), the root mean square error of the residuals (the difference between observed pCO_2 values from ice cores and reconstructed pCO_2 from foraminiferal B/Ca using the variable-alkalinity model) is 13 ppmv (fig. S9). If the other 26 models are considered, then all 41 values lie within error of the ice core record. Although only moderate in resolution, the record shows the change in the amplitude of the 100-ky cycle at 650 ka seen in ice cores (*23*). Our results for the past 1.4 Ma are very similar to those reported in a recently published $\delta^{11}B$ record (*11*).

Results for the Miocene and Late Pliocene support a close coupling between pCO_2 and climate (Fig. 2). Relative to today, surface waters appear to have been more acidic and pCO_2 values higher (Fig. 2, A and B) during the Early and Mid-Miocene (~20 to 15 Ma). This interval was characterized by global warmth, with little evidence for substantial (i.e., similar to modern) ice storage in Antarctica or Greenland (*3*, *14*, *24*). The highest estimates of pCO_2 occur during the Mid-Miocene Climatic Optimum (MMCO), ~16 to 14 Ma, the only interval in our record with levels higher than the 2009 value of 387 ppmv. Climate proxies indicate that the MMCO was associated with reduced ice volume and globally higher sea level (25 to 40 m) (*3*), as well as warmer surface- and deep-water temperatures (*2*, *20*). These results are consistent with foraminiferal $\delta^{11}B$ data that indicate that surface waters were more acidic ~20 Ma (*12*).

After the MMCO in the Mid-Miocene (~14 to 10 Ma), surface-water pH increased and pCO_2 decreased by ~200 ppmv. This pattern mirrors long-term trends in $\delta^{18}O$ records and is correlated with the appearance and growth of ice in both hemispheres, consistent with CO_2 driving this transition. Global cooling appears to have begun at ~14.2 Ma (*2*), and subsequent glacial expansion drove a 0.7 to 1.0 per mil increase in seawater and benthic foraminiferal $\delta^{18}O$ (*25*), as well as a lowering of sea level (~40 ± 15 m) (*3*). In the Northern Hemisphere, this fall in pCO_2 coincides with the onset of perennial Arctic sea ice cover (*26*), the development of substantial ice storage (*14*), and the first Miocene occurrence of ice-rafted debris in the North Atlantic, indicating that glaciers reached sea level (*24*). In the Southern Hemisphere, decreasing pCO_2 is associated with the change from wet- to cold-based alpine glaciers in the McMurdo Dry Valleys (*27*), the transition to cold polar conditions and the growth of ice on West Antarctica (*28*), and the re-initiation of a large ice sheet on East Antarctica (*2*, *29*).

During the Late Miocene (~10 to 7 Ma), seawater pH was relatively high, and pCO_2 was low and stable (~220 ppmv). Small ice sheets on West Antarctica and in the Northern Hemisphere are thought to have expanded while temperatures cooled (*13*). In the latest Miocene (~7 to 5 Ma), pH and pCO_2 exhibit large-amplitude variations, although the trends are poorly defined. This interval has been interpreted as generally being warm, with interglacials representing complete deglaciation of marine-based regions of Antarctica (*30*), consistent with the limited data on our pCO_2 curve.

Our B/Ca record indicates a large increase in pH and a fall in pCO_2 (~150 ppmv) during the Late Pliocene (~3.4 to 2.4 Ma) (Fig. 2, C and D). This evidence for a decline in pCO_2 coincident with the intensification of glaciation is consistent with the hypothesis that pCO_2 was the major driver of ice growth at this time. Model simulations also support the idea that changing pCO_2, and not ocean heat transport, triggered glaciation (*31*). Comparison with other records indicates that decreasing pCO_2 is synchronous with the intensification of continental glaciation in the Northern and Southern Hemispheres, as indicated by increased foraminiferal $\delta^{18}O$ (*32*), the onset of ice rafting in the North Pacific, and increased rates of ice rafting in the North Atlantic (*24*, *33*) and Southern Ocean (*34*). In addition, the interval of low pCO_2 at ~2.5 Ma is associated with the onset of large-amplitude (glacial-interglacial) cycles in deep-sea oxygen isotope records (*32*).

These results show that changes in pCO_2 and climate have been coupled during major glacial transitions of the past 20 My, just as they have

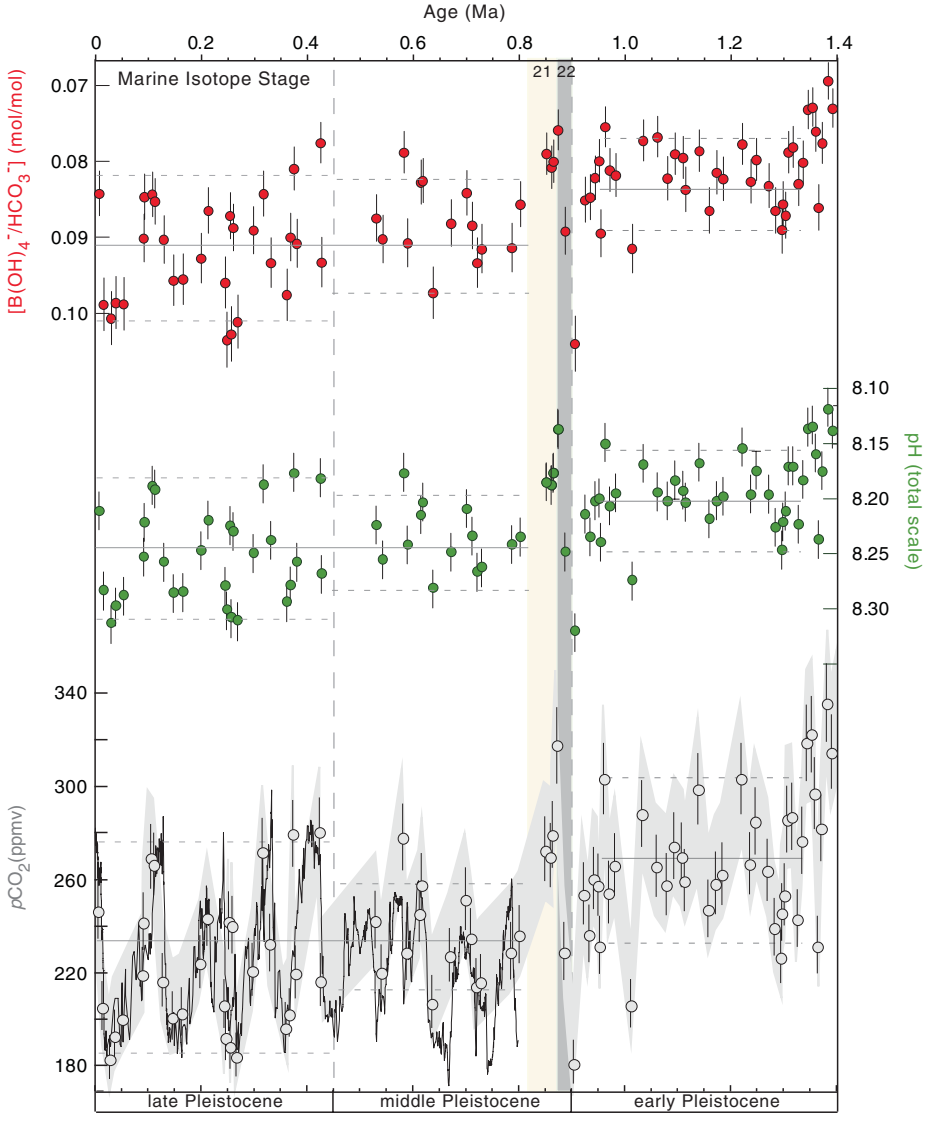

Fig. 1. $B(OH)_4^-/HCO_3^-$ ratios, pH, and pCO_2 from 0 to 1.4 Ma from B/Ca ratios of surface-dwelling foraminifera compared with Antarctic ice core data (solid line) (*23*). Data are mean ± average σ. There is a 3.5% analytical uncertainty in B/Ca ratios (average 1σ), based on analyses of replicate samples (table S8), and a 4% uncertainty in reconstructed seawater $B(OH)_4^-/HCO_3^-$ ratios, based on 78 paired measurements of *G. ruber* and *G. sacculifer* (table S9). This uncertainty in $B(OH)_4^-/HCO_3^-$ equates to a 10- to 20-ppmv uncertainty (1σ) in pCO_2 (~5 to 6%) and a 0.02 uncertainty in pH (~0.2%). The gray shaded region brackets all calculated pCO_2 values. Gray circles are for a model with a value similar to the average of all 28 models. Vertical dashed lines show Early-to-Mid Pleistocene and Mid-to-Late Pleistocene boundaries. Horizontal solid and dashed lines approximately mark shifts in mean and amplitude of values for a model shown in gray. For comparison, $\delta^{11}B$-based pCO_2 estimates indicate pCO_2 of ~220 to 300 ppmv from 0.8 to 1.4 Ma (*11*).

been over the last 0.8 My, supporting the hypothesis that greenhouse gas forcing was an important modulator of climate over this interval via direct and indirect effects. Variations in pCO_2 affect the radiative budget and energy balance of the planet. Such changes will inevitably have consequences for temperature, the hydrologic cycle, heat transport, and the accumulation and ablation of sea ice and glacial ice. The data presented here do not preclude alternative mechanisms for driving climate change over the past 20 Ma. However, they do indicate that changes in pCO_2 were closely tied to the evolution of climate during the Middle and Late Miocene and the Late Pliocene glacial intensification, and therefore, it is logical to deduce that pCO_2 played an important role in driving these transitions. High-resolution records of pCO_2 and other climate parameters should help to resolve whether pCO_2 was a trigger and/or feedback (or both).

These results provide some constraints on pCO_2 thresholds for the advance and retreat of continental ice sheets in the past, which is also relevant in the context of anthropogenic climate change because it is uncertain how continental ice sheets will respond over the coming centuries to increased levels of pCO_2 (*1*). By comparing our reconstruction to the published data sets described above, we are able to estimate past thresholds for the buildup of ice in different regions. When pCO_2 levels were last similar to modern values (that is, greater than 350 to 400 ppmv), there was little glacial ice on land or sea ice in the Arctic, and a marine-based ice mass on Antarctica was not viable. A sea ice cap on the Arctic Ocean and a large permanent ice sheet were maintained on East Antarctica when pCO_2 values fell below this threshold. Lower levels were necessary for the growth of large ice masses on West Antarctica (~250 to 300 ppmv) and Greenland (~220 to 260 ppmv). These values are lower than those indicated by a recent modeling study, which suggested that the threshold on East Antarctica may have been three times greater than in the Northern Hemisphere (*35*).

This work may support a relatively high climate sensitivity to pCO_2. pCO_2 values associated with major climate transitions of the past 20 Ma are similar to modern levels. During the Mid-Miocene, when pCO_2 was apparently grossly similar to modern levels, global surface temperatures were, on average, 3 to 6°C warmer than in the present (*2*, *25*). We suggest that the Mid-Miocene may be a useful interval to study to understand what effect sustained high pCO_2 levels (i.e., a climate in equilibrium with near-modern pCO_2 values) may have on climate.

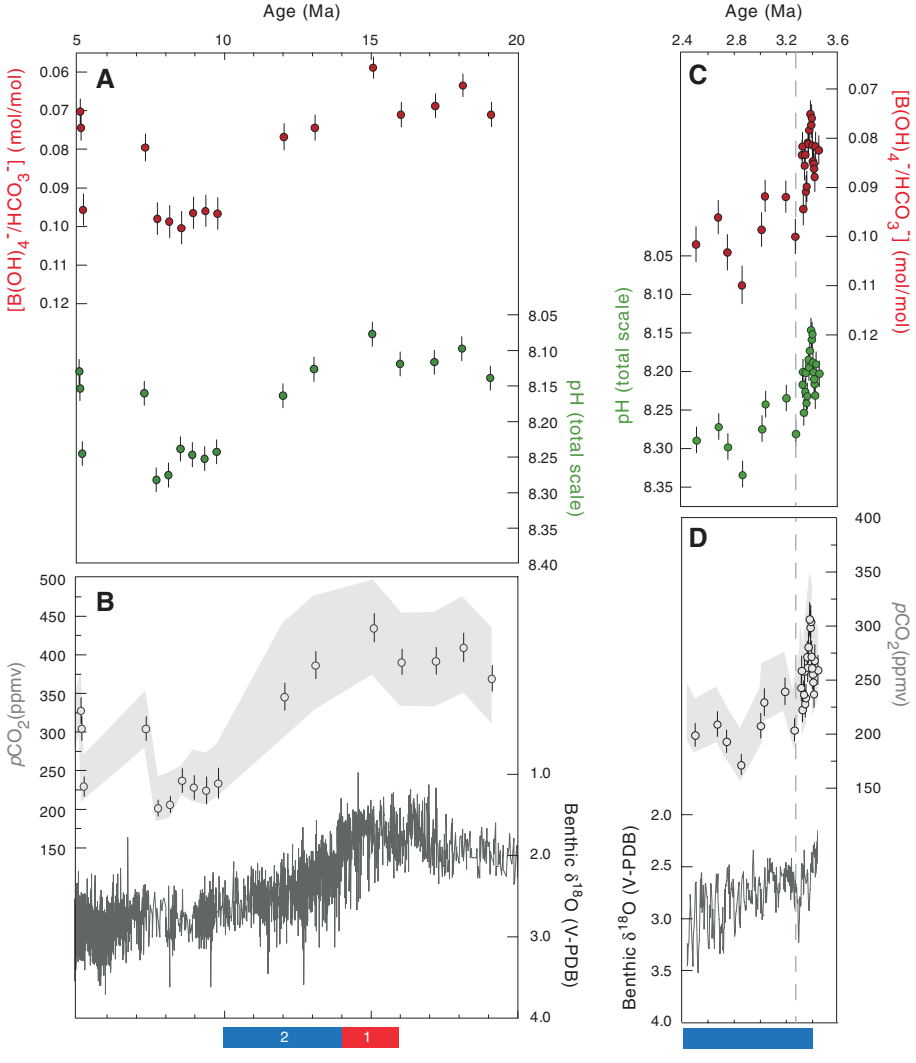

Fig. 2. pCO_2 for Miocene and Late Pliocene from B/Ca ratios of surface-dwelling foraminifera compared with climate records. Error bars are the same as in Fig. 1. The gray shaded region brackets all calculated pCO_2 values. Gray circles are for a model with a value similar to the average of all 28 models. (**A**) $B(OH)_4^-/HCO_3^-$ ratios and pH for 20 to 5 Ma. (**B**) pCO_2 and compilation of benthic foraminiferal $\delta^{18}O$ (*14*) for 20 to 5 Ma. The numbered bars at the bottom of the panel denote the timing of: (1) the MMCO (*2*, *3*, *14*, *20*, *24*) and (2) Mid-Miocene glacial expansion (*2*, *3*, *8*, *14*, *24*–*29*). (**C**) $B(OH)_4^-/HCO_3^-$ ratios and pH for 3.4 to 2.4 Ma. (**D**) pCO_2 and benthic foraminiferal $\delta^{18}O$ (*32*) for 3.4 to 2.4 Ma. The dark blue bar at the bottom of the panel denotes the reported timing of Late Pliocene glacial expansion (*14*, *24*, *32*–*34*). V-PDB, Vienna Pee Dee belemnite.

References and Notes

1. Intergovernmental Panel on Climate Change, *Climate Change 2007: The Physical Science Basis. Contribution of Working Group I to the Fourth Assessment Report of the Intergovernmental Panel on Climate Change*, S. Solomon *et al.*, Ed. (Cambridge Univ. Press, Cambridge, 2007).
2. A. E. Shevenell, J. P. Kennett, D. W. Lea, *Science* **305**, 1766 (2004).
3. K. G. Miller *et al.*, *Science* **310**, 1293 (2005).
4. G. Haug, D. Sigman, R. Tiedemann, T. Pedersen, M. Sarnthein, *Nature* **401**, 779 (1999).
5. G. Haug, R. Tiedemann, *Nature* **393**, 673 (1998).
6. D. M. Sigman, S. L. Jaccard, G. H. Haug, *Nature* **428**, 59 (2004).
7. E. Vincent, W. Berger, in *The Carbon Cycle and Atmospheric CO_2: Natural Variations Archean to Present*, vol. 32, E. Sundquist, W. Broecker, Eds. (Geophys. Monogr. Ser., AGU, Washington, DC, 1985), pp. 455–468.
8. A. Holbourn, W. Kuhnt, M. Schulz, H. Erlenkeuser, *Nature* **438**, 483 (2005).
9. D. Hodell, F. Woodruff, *Paleoceanography* **9**, 405 (1994).
10. M. Pagani, J. C. Zachos, K. H. Freeman, B. Tipple, S. Bohaty, *Science* **309**, 600 (2005); published online 16 June 2005 (10.1126/science.1110063).
11. B. Hönisch, N. G. Hemming, D. Archer, M. Siddall, J. F. McManus, *Science* **324**, 1551 (2009).
12. A. Spivack, C. You, H. Smith, *Nature* **363**, 149 (1993).
13. P. N. Pearson, M. R. Palmer, *Nature* **406**, 695 (2000).
14. J. Zachos, M. Pagani, L. Sloan, E. Thomas, K. Billups, *Science* **292**, 686 (2001).
15. J. Yu, H. Elderfield, B. Hönisch, *Paleoceanography* **22**, PA2202 (2007).
16. A. V. Federov *et al.*, *Science* **312**, 1485 (2006).
17. M. W. Wara, A. C. Ravelo, M. L. Delaney, *Science* **309**, 758 (2005); published online 23 June 2005 (10.1126/science.1112596).
18. S. Nathan, R. Leckie, *Palaeogeogr. Palaeoclimatol. Palaeoecol.* **274**, 140 (2009).
19. M. Medina-Elizalde, D. Lea, *Science* **310**, 1009 (2005); published online 13 October 2005 (10.1126/science.1115933).
20. B. Flower, J. Kennett, *Paleoceanography* **8**, 811 (1993).
21. Materials and methods are available as supporting material on *Science* Online.
22. D. Lemarchand, J. Gaillardet, E. Lewin, C. Allegre, *Chem. Geol.* **190**, 123 (2002).
23. D. Luthi *et al.*, *Nature* **453**, 379 (2008).
24. T. Wolf-Welling, M. Cremer, S. O'Connell, A. Winkler, J. Thiede, in *Proceedings of Ocean Drilling Program, Scientific Results*, vol. 151, J. Thiede, A. Myhre, J. Firth,

G. Johnson, W. Ruddiman, Eds. (Ocean Drilling Program, College Station, TX, 1996), pp. 515–568.
25. K. Billups, D. Schrag, *Earth Planet. Sci. Lett.* **209**, 181 (2003).
26. A. Krylov *et al.*, *Paleoceanography* **23**, PA1S06 (2008).
27. A. R. Lewis *et al.*, *Proc. Natl. Acad. Sci. U.S.A.* **105**, 10676 (2008).
28. T. Naish *et al.*, *Nature* **458**, 322 (2009).
29. B. Flower, J. Kennett, *Paleoceanography* **10**, 1095 (1995).
30. T. Naish *et al.*, paper presented at the International Symposium on Antarctic Earth Sciences, Santa Barbara, CA, 26 to 31 August 2007.
31. D. J. Lunt, G. L. Foster, A. M. Haywood, E. J. Stone, *Nature* **454**, 1102 (2008).
32. L. E. Lisiecki, M. E. Raymo, *Paleoceanography* **20**, PA1003 (2005).
33. L. Krissek, in *Proceedings of the Ocean Drilling Program, Scientific Results*, vol. 145, D. Rea, I. Basov, D. Scholl, J. Allan, Eds. (Ocean Drilling Program, College Station, TX, 1995), pp. 179–194.
34. E. Cowan, in *Proceedings of the Ocean Drilling Program, Scientific Results*, vol. 178, P. Barker, A. Camerlenghi, G. Acton, Eds. (Ocean Drilling Program, College Station, TX, 2001), pp. 1–22.
35. R. M. DeConto *et al.*, *Nature* **455**, 652 (2008).
36. We thank K. Caldeira, H. Elderfield, J. Eiler, T. Naish, D. Sigman, anonymous reviewers, and the editor for their comments on this work, which substantially improved the manuscript. We also thank J. Booth, E. Khadun, O. Shorttle, L. Thanalasundaram, and A. Bufe for invaluable assistance with sample preparation; L. Booth, J. Day, and M. Greaves (supported by grant NE/F004966/1) for technical assistance; L. Lisiecki for assistance with the age model; and S. Crowhurst, A. Gagnon, S. John, N. Meckler, B. Passey, N. Thiagarajan, and J. Yu for discussing this work. Support was provided to A.K.T. by UCLA, National Environmental Research Council (NERC) (fellowship NE/D009049/1), and Magdalene College; to C.D.R. by NERC (studentship NER/S/A/2006/14070); and to R.A.E. by a Caltech Chancellors Postdoctoral Scholarship. Samples for this study were obtained from the Godwin Laboratory sample archives and the Ocean Drilling Program.

Supporting Online Material
www.sciencemag.org/cgi/content/full/1178296/DC1
Materials and Methods
Figs. S1 to S9
Tables S1 to S12
References

26 June 2009; accepted 28 September 2009
Published online 8 October 2009;
10.1126/science.1178296
Include this information when citing this paper.

Indirect Emissions from Biofuels: How Important?

Jerry M. Melillo,[1]* John M. Reilly,[2] David W. Kicklighter,[1] Angelo C. Gurgel,[2,3] Timothy W. Cronin,[1,2] Sergey Paltsev,[2] Benjamin S. Felzer,[1,4] Xiaodong Wang,[2,5] Andrei P. Sokolov,[2] C. Adam Schlosser[2]

A global biofuels program will lead to intense pressures on land supply and can increase greenhouse gas emissions from land-use changes. Using linked economic and terrestrial biogeochemistry models, we examined direct and indirect effects of possible land-use changes from an expanded global cellulosic bioenergy program on greenhouse gas emissions over the 21st century. Our model predicts that indirect land use will be responsible for substantially more carbon loss (up to twice as much) than direct land use; however, because of predicted increases in fertilizer use, nitrous oxide emissions will be more important than carbon losses themselves in terms of warming potential. A global greenhouse gas emissions policy that protects forests and encourages best practices for nitrogen fertilizer use can dramatically reduce emissions associated with biofuels production.

Expanded use of bioenergy causes land-use changes and increases in terrestrial carbon emissions (*1*, *2*). The recognition of this has led to efforts to determine the credit toward meeting low carbon fuel standards (LCFS) for different forms of bioenergy with an accounting of direct land-use emissions as well as emissions from land use indirectly related to bioenergy production (*3*, *4*). Indirect emissions occur when biofuels production on agricultural land displaces agricultural production and causes additional land-use change that leads to an increase in net greenhouse gas (GHG) emissions (*2*, *4*). The control of GHGs through a cap-and-trade or tax policy, if extended to include emissions (or credits for uptake) from land-use change combined with monitoring of carbon stored in vegetation and soils and enforcement of such policies, would eliminate the need for such life-cycle accounting (*5*, *6*). There are a variety of concerns (*5*) about the practicality of including land-use change emissions in a system designed to reduce emissions from fossil fuels, and that may explain why there are no concrete proposals in major countries to do so. In this situation, fossil energy control programs (LCFS or carbon taxes) must determine how to treat the direct and indirect GHG emissions associated with the carbon intensity of biofuels.

The methods to estimate indirect emissions remain controversial. Quantitative analyses to date have ignored these emissions (*1*), considered those associated with crop displacement from a limited area (*2*), confounded these emissions with direct or general land-use emissions (*6*–*8*), or developed estimates in a static framework of today's economy (*3*). Missing in these analyses is how to address the full dynamic accounting of biofuel carbon intensity (CI), which is defined for energy as the GHG emissions per megajoule of energy produced (*9*), that is, the simultaneous consideration of the potential of net carbon uptake through enhanced management of poor or degraded lands, nitrous oxide (N_2O) emissions that would accompany increased use of fertilizer, environmental effects on terrestrial carbon storage [such as climate change, enhanced carbon dioxide (CO_2) concentrations, and ozone pollution], and consideration of the economics of land conversion. The estimation of emissions related to global land-use change, both those on land devoted to biofuel crops (direct emissions) and those indirect changes driven by increased demand for land for biofuel crops (indirect emissions), requires an approach to attribute effects to separate land uses.

We applied an existing global modeling system that integrates land-use change as driven by multiple demands for land and that includes dynamic greenhouse gas accounting (*10*, *11*). Our modeling system, which consists of a computable general equilibrium (CGE) model of the world economy (*10*, *12*) combined with a process-based terrestrial biogeochemistry model (*13*, *14*), was used to generate global land-use scenarios and explore some of the environmental consequences of an expanded global cellulosic biofuels program over the 21st century. The biofuels scenarios we focus on are linked to a global climate policy to control GHG emissions from industrial and fossil fuel sources that would, absent feedbacks from land-use change, stabilize the atmosphere's CO_2 concentration at 550 parts per million by volume (ppmv) (*15*). The climate policy makes the use of fossil fuels more expensive, speeds up the introduction of biofuels, and ultimately increases the size of the biofuel industry, with additional effects on land use, land prices, and food and forestry production and prices (*16*).

We considered two cases in order to explore future land-use scenarios: Case 1 allows the conversion of natural areas to meet increased demand for land, as long as the conversion is profitable; case 2 is driven by more intense use of existing managed land. To identify the total effects of biofuels, each of the above cases is compared with a scenario in which expanded biofuel use does not occur (*16*). In the scenarios with increased biofuels production, the direct effects (such as changes in carbon storage and N_2O emissions) are estimated only in areas devoted to biofuels. Indirect effects are defined as the differences between the total effects and the direct effects.

At the beginning of the 21st century, ~31.5% of the total land area (133 million km^2) was in

[1]The Ecosystems Center, Marine Biological Laboratory (MBL), 7 MBL Street, Woods Hole, MA 02543, USA. [2]Joint Program on the Science and Policy of Global Change, Massachusetts Institute of Technology (MIT), 77 Massachusetts Avenue, MIT E19-411, Cambridge, MA 02139-4307, USA. [3]Department of Economics, University of São Paulo, Ribeirão Preto 4EES, Brazil. [4]Department of Earth and Environmental Sciences, Lehigh University, 31 Williams Drive, Bethlehem, PA 18015, USA. [5]School of Public Administration, Zhejiang University, Hangzhou 310000, Zhejiang Province, People's Republic of China (PRC).

*To whom correspondence should be addressed. E-mail: jmelillo@mbl.edu